

Poh Gangkai (Orcid ID: 0000-0002-5775-2006)
Slavin James, A. (Orcid ID: 0000-0002-9206-724X)
Jia Xianzhe (Orcid ID: 0000-0002-8685-1484)
Sun Wei-Jie (Orcid ID: 0000-0001-5260-658X)
Raines Jim, M (Orcid ID: 0000-0001-5956-9523)
Imber Suzanne, Mary (Orcid ID: 0000-0001-7917-8087)
DiBraccio Gina, A. (Orcid ID: 0000-0002-2778-4998)
Gershman Daniel, J (Orcid ID: 0000-0003-1304-4769)

Transport of Mass and Energy in Mercury's Plasma Sheet

Gangkai Poh¹, James A. Slavin¹, Xianzhe Jia¹, Wei-Jie Sun¹, Jim M. Raines¹, Suzanne M. Imber², Gina A. DiBraccio³, Daniel J. Gershman⁴

¹ Department of Climate and Space Sciences and Engineering, University of Michigan, Ann Arbor, Michigan, USA,

² Department of Physics and Astronomy, University of Leicester, Leicester, United Kingdom,

³ Solar System Exploration Division, NASA Goddard Space Flight Center, Greenbelt, Maryland, USA,

⁴ Heliophysics Science Division, NASA Goddard Space Flight Center, Greenbelt, Maryland, USA.

This is the author manuscript accepted for publication and has undergone full peer review but has not been through the copyediting, typesetting, pagination and proofreading process, which may lead to differences between this version and the [Version of Record](#). Please cite this article as doi: [10.1029/2018GL080601](https://doi.org/10.1029/2018GL080601)

Abstract:

We examined the transport of mass and energy in Mercury's plasma sheet (PS) using MESSENGER magnetic field and plasma measurements obtained during 759 PS crossings. Regression analysis of proton density and plasma pressure shows a strong linear relationship. We calculated the polytropic index γ for Mercury's PS to be ~ 0.687 , indicating that the plasma in the tail PS behaves non-adiabatically as it is transported sunward. Using the average magnetic field intensity of Mercury's tail lobe as a proxy for magnetotail activity level, we demonstrated that γ is lower during active time periods. A minimum in γ was observed at $R \sim 1.4 R_M$, which coincides with previously observed location of Mercury's substorm current wedge. We suggest that the non-adiabatic behavior of plasma as it is transported into Mercury's near-tail region is primarily driven by particle precipitation and particle scattering due to large loss cone and particle acceleration effect, respectively.

1. Introduction

In situ magnetic field and plasma measurements observed by MESSENGER allowed us to understand the dynamics and structure of Mercury's magnetotail [Slavin *et al.*, 2012] and plasma sheet (PS) [DiBraccio *et al.*, 2015a; Poh *et al.*, 2017a; Rong *et al.*, 2018]. Large-scale statistical studies have shown that processes occurring in Mercury's magnetotail are qualitatively similar to Earth's, despite the differences in spatial and temporal scales, upstream conditions and internal plasma compositions [Raines *et al.*, 2011; Gershman *et al.*, 2014; Poh *et al.*, 2017b]. Mass, energy and magnetic flux are transported from Mercury's dayside magnetopause to its nightside magnetotail via an Earth-like Dungey cycle [Slavin *et al.*, 2010; Imber and Slavin, 2017]. The cycle is completed by the return flow of mass, energy and flux towards Mercury driven by

magnetic reconnection in Mercury's PS [*Slavin et al.*, 2009; *Sundberg et al.*, 2012; *Sun et al.*, 2015; *DiBraccio et al.*, 2015b; *Smith et al.*, 2017; *Zhong et al.*, 2018].

In order to understand mass, momentum and energy transport through a planetary magnetotail, it is essential to understand the sunward convection of closed flux tubes and thermodynamic properties of particles within the PS [*Siscoe*, 1983; *Baumjohann and Paschmann*, 1989]. In magnetohydrodynamics (MHD) theory, the local plasma pressure (P_i) can be expressed as:

$$P_i = \alpha n_i^\gamma \quad (1)$$

where n_i is the proton number density. α is a constant related to the specific entropy of a particular flux tube. The polytropic index γ in Equation (1) determines the type of thermodynamic process a closed flux tube experience as it is transported sunward. In an ideal, adiabatic system where there is no particle source or loss (i.e. reversible process) and no heat transfer in and out of the PS, it should be the case that $\gamma = 5/3$ or (~ 1.67). Indeed, this is the value of γ is commonly used in MHD simulations [e.g. *Jia et al.*, 2015]. If γ is less than $5/3$, it means that the plasma behaves non-adiabatically (i.e., particle gain/loss or heat transfer or both). Equation (1) can be linearized:

$$\log P_i = \gamma \log n_i + \log \alpha \quad (2)$$

γ may then be calculated by performing linear regression analysis on $\log(P_i)$ and $\log(n_i)$.

Baumjohann and Paschmann, [1989] first determined the overall value of polytropic index for the Earth's PS using AMPTE/IRM plasma data under a wide range of conditions and regions, and found it to be ~ 1.69 , which is close to $5/3$, suggesting adiabatic plasma behavior. On the other hand, using ISEE-1 data, *Huang et al.*, [1989] calculated a γ value of ~ 0.6 , which would require that the plasma on a flux tube undergoing rapid contraction as it moves planetward to cool as opposed to heat due to compression. However, this value of 0.6 is closer to that determined by *Schindler and Birn* [1982] who produced a realistic variation of pressure with radial distance by inputting a value of $\gamma = 2/3$ in the equation of state. This avoided the unrealistic order of magnitude pressure increase in near-Earth magnetotail that arises when using $\gamma = 5/3$ from ideal MHD theory [*Erickson and Wolf*, 1980]. *Spence et al.*, [1989] determined a similar result using statistical averages of plasma pressure observed in the near-Earth magnetotail region. The $2/3$ value was also used by *Kivelson and Spence*, [1988] in their modified magnetotail model while investigating the effects of finite tail width. *Borovsky et al.*, [1998] subsequently calculated γ to be ~ 1.52 using ISEE-2 data while *Pang et al.*, [2015] found a range of γ values from ~ 0.1 to 1.8 using Cluster data. More recently, *Frühhauff et al.*, [2017] obtained a γ of ~ 1.72 using THEMIS data. Taken together, these results suggest that γ for Earth's PS is highly dependent on the data set used in the analysis.

MESSENGER's measurements of ion temperature and density [*Andrews et al.*, 2007] and magnetic fields [*Anderson et al.*, 2007] during its 4 year orbital mission around Mercury provide the first opportunity to investigate the transport of mass and energy in Mercury's plasma sheet.

Here, we will describe the method used to identify these intervals of MESSENGER's encounter with Mercury's PS. Using regression and statistical analysis of the plasma measurements, we calculated an average γ of ~ 0.687 and demonstrated a relationship between γ and substorm-related phenomenon in Mercury's PS.

2. MESSENGER Dataset and Event Selection

In this study, we analyzed the full-resolution one energy scan/10s plasma [Andrews *et al.*, 2007] and 20 vectors/second magnetic field [Anderson *et al.*, 2007] measurements from MESSENGER's Fast Imaging Plasma Spectrometer (FIPS) and Magnetometer (MAG), respectively. The accuracy of our calculated polytropic index is limited by our ability to observe the plasma in a given magnetic flux tube as it travels sunward. The assumption of constant specific entropy in each flux tube becomes a significant source of uncertainty since we do not know the flux tubes' history [Zhu 1990]. As a result, noise and biases may be introduced which could influence our determination of γ at Mercury. Therefore, it is important to use the plasma measurements in its highest data resolution. However, due to its placement on the MESSENGER spacecraft, FIPS had limited field-of-view (FOV) of the full proton distribution (See Gershman *et al.*, [2013] for more details). This poses a challenge to accurately calculate the moments of the bulk plasma sheet population (i.e., plasma density and temperature) at Mercury in FIPS native resolution of 10s per full scan of all energy levels. Therefore, we chose to use the 1-minute averaged plasma moments derived from FIPS data.

We chose the Mercury Solar Magnetospheric (MSM) coordinate system for analyses performed in this study. The MSM coordinate system is centered on Mercury's internal offset dipole [Anderson *et al.*, 2011]. The X -axis is positive in the sunward direction along the Sun-Mercury line, Z -axis is positive northward parallel to Mercury's magnetic dipole moment axis, and Y -axis completes the right-handed system. To account for solar wind aberration, we rotate the MSM X - and Y -axes by the solar wind aberration angle, which was calculated on a daily basis assuming a radial solar wind speed of 400 km/s, into the new aberrated MSM (or MSM') coordinate system.

Figure 1 shows an example of MESSENGER's traversal of Mercury's PS on February 18th 2012. Panel 1 shows the energy-per-charge (E/Q) spectrogram observed by FIPS. Panel 2 shows the plasma β (i.e. thermal to magnetic pressure ratio) calculated using FIPS' plasma moments; x , y and z -components and magnitude ($|\mathbf{B}|$) of the magnetic field measurements are shown in Panels 3 – 6, respectively. The interval starts with MESSENGER in the southern tail lobe, which is characterized by the low plasma β (~ 0.05), strong $|\mathbf{B}|$ (~ 50 nT) and low levels of fluctuation predominantly in the negative B_X direction. At \sim UT12:53, MESSENGER entered the southern plasma sheet boundary layer (PSBL), which is identified by moderate $|\mathbf{B}|$ fluctuations of ~ 10 nT [e.g. Slavin *et al.*, 1985]. MESSENGER then entered the PS at \sim UT12:58 shown by the further decrease of $|\mathbf{B}|$ to ~ 15 nT, reversal of B_X across the cross-tail current sheet, presence of 0.5 – 1 keV protons and increase of β to ~ 10 . Lastly, MESSENGER exited the PS into the northern

PSBL, and subsequently into the high latitude, northern part of Mercury's dipolar, low β (~ 0.02) inner magnetotail region characterized by positive B_X and strong $|\mathbf{B}|$ of ~ 100 nT.

We visually identified a total of 759 PS crossings over four years of MESSENGER data using the following selection criteria:

1. Plasma β inside the PS and PSBL must be **greater than 0.5**.
2. A crossing of the cross-tail current sheet, identified by a clear reversal in B_X coincident with a depression in $|\mathbf{B}|$ must be present.

Plasma β has been used extensively in many magnetotail studies to identify the boundary between the PS region (including the PSBL) and tail lobe. Terrestrial studies (e.g., *Angelopoulos et al.*, [1994]) used a range of β cutoff values from 0.1 to 0.5 to identify the boundaries of Earth's PS. In this study, we adopted the criteria used by *Sun et al.*, [2016] to define Mercury's PS as the region with $\beta \geq 0.5$. The vertical lines in Figure 1 denotes the PS boundary set by this criteria.

3. Analysis

3.1 Polytropic Index

Figure 2 shows all P_i vs. n_i measurements observed during the 759 PS crossings identified in this study. Note that both P_i and n_i -axes have logarithmic scales. As shown in Figure 2, MESSENGER measured a large range of P_i and n_i during the PS encounters, ranging from 0.06 –

7nPa and $0.08 - 30\text{cm}^{-3}$, respectively. Note that the high pressure and density measurements correspond to measurements made in the PS, while the low pressure and density measurements correspond to those measured in the PSBL. Figure 2 also clearly shows a linear relationship between the logarithmic values of P_i and n_i as indicated by the linearized equation of state (Equation 2). Correlation analysis yields a correlation coefficient (r) of ~ 0.684 , which indicates that there is a linear relationship between $\log(P_i)$ and $\log(n_i)$, consistent with a single, well-constrained polytropic exponent.

Since this is a two-dimensional data set, we performed the Deming regression analysis [Deming, 1943] on the P_i vs. n_i measurements, which accounts for errors in both variables (P_i and n_i) to compute the line of best fit. We also used the jackknife method [Linnet, 1990] to estimate the errors in the slope and y-intercept of the regression line. The regression analysis yields a regression coefficient (i.e., polytropic index γ) of $\sim 0.687 \pm 0.008$. Since the calculated value of γ is much smaller than $5/3$ (~ 1.67), our result suggests that the plasma inside a contracting flux tube in the PS cools as it is transported sunward towards Mercury. This result also indicates that the plasma pressure in Mercury's inner magnetotail is lower than that predicted from the equation of state with $\gamma = 5/3$. There appears to be a net energy and particles lost from the flux tube during the convection process in Mercury's inner magnetotail. Implications of these results will be further discussed in the Discussion section.

3.2 Dependence of Magnetotail Activity Level

We further examined the dependence of γ on the level of magnetotail activities. Earlier terrestrial studies on the determination of γ for Earth's PS (*Frühhauff et al.*, [2017] and references therein) shows the importance of separating the P_i and n_i data set according to the activity level (i.e., quiet and active times) of the terrestrial magnetotail. A similar index based on the level of magnetic fluctuations observed within Mercury's magnetosphere was developed by *Anderson et al.*, [2013]. Here, we used the average magnetic field intensity of Mercury's tail lobe ($|\mathbf{B}_{\text{lobe}}|$) instead for each identified PS crossing event as a proxy for activity level in Mercury's magnetotail. We assumed that $|\mathbf{B}_{\text{lobe}}|$ does not have spatial or temporal dependence during each PS crossing. The use of $|\mathbf{B}_{\text{lobe}}|$ as a first order approximation for Mercury's magnetotail activity is suitable because $|\mathbf{B}_{\text{lobe}}|$ tends to be higher during the growth and expansion phase (or active periods) of the substorm process and lower during quiet periods [e.g., *Sun et al.*, 2015; *Imber and Slavin*, 2017].

Figure 3a shows the P_i and n_i diagram similar to Figure 2; the colors associated with each P_i and n_i measurements represents $|\mathbf{B}_{\text{lobe}}|$ for the corresponding PS crossing. It is clear that there are two different groups of measurements distinguished by $|\mathbf{B}_{\text{lobe}}|$. It is expected that higher magnetic field intensity in the tail lobe leads to higher plasma pressure in Mercury's PS. Using a range of $|\mathbf{B}_{\text{lobe}}|$ threshold values, we determined that a threshold value of 60 nT best define the two subsets of measurements representing quiet and active conditions. We separated the entire data set into two subsets for quiet (i.e. $|\mathbf{B}_{\text{lobe}}| < 60$ nT) and active (i.e. $|\mathbf{B}_{\text{lobe}}| > 60$ nT) magnetotail as shown in Figure 3b and 3c, respectively. The regression analyses yield a γ value of $\sim 0.636 \pm 0.008$ and

0.58 ± 0.02 for the quiet and active data subsets, respectively. The correlation coefficient is ~ 0.68 for both subsets, indicating successful regression analyses. Our results show that γ is $\sim 13\%$ smaller during active than quiet times, which suggests that planetward convection is less adiabatic and more particles and energy are lost from the flux tube when Mercury's magnetotail is more active (i.e. during substorms).

3.3 Downtail Variation of γ in Mercury's Plasma Sheet

We examined the radial distance from Mercury (R) dependencies of the polytropic index γ . Using only measurements within $\pm 1 R_M$ centered on the noon-midnight meridian, we binned the plasma measurements into radial bins of $0.1 R_M$ from $R = 1.2 R_M$ to $2.6 R_M$ and compute γ for each bin using the regression technique discussed in Section 3.1. The calculated γ as a function of R is shown in the top panel of Figure 4. The error bars represent the standard errors of the calculated regression line parameters.

Our results show that the value of γ remains constant at ~ 0.65 between $R = 2 - 2.4 R_M$. However, γ decreases steadily with decreasing radial distance from Mercury between $1.5 R_M$ until it reaches a minimum at $R \sim 1.4 R_M$ with $\gamma \sim 0.45$ before increasing to ~ 0.75 at $R \sim 1.2 R_M$. The relative size of the error bars and constant r for the measurements in all R bins (red line) at ~ 0.7 indicates that the minima in γ is unlikely to be the results of observational bias. The location of the minima in γ coincides with the location of Mercury's substorm current wedge (SCW)

identified by *Poh et al.*, [2017b]. A similar minimum in γ as a function of R was also observed in the terrestrial study by *Frühhauff et al.*, [2017]. They suggested a connection between the decrease of γ and the flow-braking region typically observed at $X \sim -15 R_M$ (e.g., *Shiokawa et al.*, [1997]). Our result also suggests a similar connection between the observed decrease in γ and the location of the flow-braking region in Mercury's inner magnetotail.

4. Summary and Discussion

MESSENGER observations of 759 crossings of Mercury's PS were examined and our results can be summarized as follows:

- I. We calculated the average value of γ for Mercury's PS to be ~ 0.687 .
- II. We demonstrated that γ is lower during active times than quiet times.
- III. The observed minimum in γ at $R \sim 1.4 R_M$ indicates a relationship between decreases in γ and location of the flow braking region in Mercury's inner magnetotail.

The polytropic index γ determines the thermodynamic process a closed flux tube experience as it is transported sunward. Our regression analysis of FIPS plasma measurements yielded a polytropic index γ of ~ 0.687 (or $\sim 2/3$) for Mercury's PS, which is smaller than the adiabatic polytropic index of $5/3$. This result suggests that the plasma within the contracting, planetward moving flux tube "cools", indicating net particle and energy loss, as the flux tube is transported into Mercury's low- β inner magnetotail region. Our calculated γ value is consistent with the $\gamma =$

$2/3$ value determined by some terrestrial studies based on their Earth's magnetospheric model [Schindler and Birn, 1982; Kivelson and Spence, 1988] and observations [Spence et al., 1989; Huang et al., 1989]. Kivelson and Spence [1988] concluded that the effects of finite tail width and loss of particles through precipitation could account for the observed lower plasma pressure (i.e. $\gamma = 2/3$) [Spence et al., 1989] in the near-tail region under the condition of steady state convection occurring in the magnetotail. The agreement between both our observations and simulation results from the Kivelson and Spence, [1988] magnetospheric model strongly suggests that similar mechanisms might be occurring in Mercury's PS that would result in our observation of $\gamma \sim 0.687$, which is not surprising considering the strength of Mercury's global magnetic field and the typical ion gyroradius (~ 380 km [DiBraccio et al., 2015b]) relative to the system size.

The two primary sink mechanisms for particles in Mercury's PS are: (1) Particle precipitation due to large loss cone, and (2) non-adiabatic particle scattering due to strong acceleration processes. Earlier studies have shown that the loss cone for Mercury's magnetospheric cusp is uniquely large (e.g., Goldstein et al., [1981]; Raines et al., [2014]). The equatorial loss cone for Mercury's nightside magnetosphere ranges from $\sim 13^\circ$ to 23° , as compared to Earth's loss cone of $< 3^\circ$ beyond geosynchronous orbit ($\sim 6 R_E$) [Baumjohann and Treumann, 1996]. As a result of Mercury's large loss cone, particles with sufficiently small pitch angles are likely to precipitate onto Mercury's high latitude nightside surface and become lost from the flux tubes, instead of mirroring at the high latitude mirror point and undergoing several bounce motions to become "trapped" within the flux tube, as in the case of Earth. This effect is further enhanced by

Mercury's offset dipole magnetic field with more plasma sheet particle loss in the southern hemisphere surface [Korth *et al.*, 2014]. Furthermore, at Earth, outflow from the terrestrial ionosphere serves as a significant source of magnetospheric plasma for the terrestrial PS [Chappell *et al.*, 1987], continually replenishing flux tubes as they propagate earthward. In contrast, Mercury's lack of an ionosphere means there is only a low flux of plasma, produced by photo-ionization and subsequent acceleration of exospheric ions, drifting into Mercury's magnetotail. This source is insufficient to refill flux tubes depleted by constant precipitation as they propagate into Mercury's inner magnetotail. Through this mechanism, Mercury's large loss cone contributes to the non-adiabatic behavior of plasma within a closed flux tube observed in this study.

Another reason for non-adiabatic plasma behavior at Mercury is scattering of particles due to the complex set of acceleration processes occurring in Mercury's magnetotail [e.g. Zelenyi *et al.*, 2007]. Solar wind and planetary ions in Mercury's PS are known to have large gyroradius relative to the scale length of magnetic field variations due to Mercury's weak intrinsic magnetic field. The influence of centrifugal force on particle motion becomes important in Mercury's plasma sheet due to finite gyro-radius effects [Delcourt, 1996], thereby accelerating particles and result in non-adiabatic Speiser-type orbits [Delcourt *et al.*, 2003] across magnetospheric regions. At Mercury, particles were also observed to be energized and accelerated near the X-line by magnetic reconnection [Zhong *et al.*, 2018], and reconnection-related phenomena, such as dipolarization fronts [Sun *et al.*, 2017; Dewey *et al.*, 2017]. Particle acceleration could result in

the chaotic and non-adiabatic motion of particles [Buchner and Zelenyi, 1989], thereby resulting in the loss of particles within the flux tube during compressional convection and subsequent transport into another magnetospheric region, impact onto Mercury's nightside surface or shadowing of the magnetopause. Therefore, the scattering of particles due to particle acceleration processes providing another plausible explanation of why $\gamma \sim 2/3$ (instead of $5/3$) in Mercury's PS.

Our analysis also shows that γ is lower during PS crossings when higher $|\mathbf{B}_{\text{lobe}}|$ were observed. During active magnetic reconnection, particle scattering effects play an even more important role in the transport of particles from one magnetospheric region to another. Particles energized and accelerated by magnetic reconnection and dipolarization fronts [Sun *et al.*, 2017; 2018] execute a larger, more chaotic gyro-motion and are more likely to be lost from the flux tubes into other magnetospheric regions or shadowing of the nightside magnetopause. Furthermore, the increase of B_z in the PS during substorm expansion phase increases the nightside loss cone angle, resulting in more particles being lost due to particle precipitation onto Mercury's nightside surface. The increased effects of particle scattering and loss cone precipitation during active reconnection contribute to enhanced loss of particles and hence, lower γ , during active time periods.

Analysis of the polytropic index γ with radial distance shows a minimum in γ at $R \sim 1.4 R_M$. Similar feature in the radial profile of γ at Earth was reported by Fröhlich *et al.*, [2017], who suggested a connection between γ and the flow-braking region in the near-Earth magnetotail

region. At Mercury, this minimum also occurs near the region where *Poh et al.*, [2017b] reported observations of Mercury's SCW. When the reconnection rate at Mercury's dayside magnetopause [*DiBraccio et al.*, 2013] is faster than the reconnection rate in the magnetotail, magnetic flux builds up in the two tail lobes. Substorm onset occurs during a sudden unloading of lobe magnetic flux [*Slavin et al.*, 2010] in the highly-stretched, thin plasma sheet, which launches Alfvénic Bursty Bulk Flows (BBFs), carrying dipolarized flux tubes towards Mercury. The sunward fast flows brake due to the tailward pressure gradient force as it encounters Mercury's low- β inner magnetotail region, resulting in the diversion of plasma flow and ultimately the loss of ions from the flux tubes. The additional loss of particles due to flow braking exacerbates the problem of particle loss due to scattering and large loss cone, hence explaining the observed decrease (and minima) of γ around the flow breaking region in Mercury's magnetotail. These plasma-depleted flux tubes (or bubbles) [*Chen and Wolf*, 1993] with low specific entropy will continue to propagate further into Mercury's inner-tail region until the increase (decrease) in plasma pressure (flux tube volume) stops its motion. This flux tube transport process is similar to that observed at Earth [e.g. *Sergeev et al.*, 1996].

Looking into the future, the upcoming Bepi-Colombo mission, consisting of the Mercury Magnetospheric Orbiter (MMO) and Mercury Planetary Orbiter (MPO), will take our understanding of the transport of mass and energy in Mercury's magnetotail to the next level. The Mercury Ion Analyzer (MIA) and Search for Exospheric Refilling and Emitted Natural Abundances (SERENA) instrument suite will be able to obtain the full 3-D distribution function

[*Saito et al.*, 2010] and measures particle precipitation [*Orsini et al.*, 2010], respectively, allowing us to accurately determine the plasma moments in each magnetotail regions. Advances in data sets measured by Bepi-Colombo will greatly improve our understanding of how mass and energy is transported in Mercury's magnetotail.

Acknowledgements

Data sets analyzed in this study are archived with the NASA Planetary Data System (PDS) (<https://pds.nasa.gov/>). The authors acknowledged support provided by NASA Discovery Data Analysis Program (DDAP) grants NNX15K88G, NNX15AL01G and NNX16AJ05G, Heliophysics Supporting Research (HSR) NNX15AJ68G, Living with a Star NNX16AJ67G, and Solar System Workings (SSW) Program grant NNX15AH28G to the University of Michigan.

Figures:

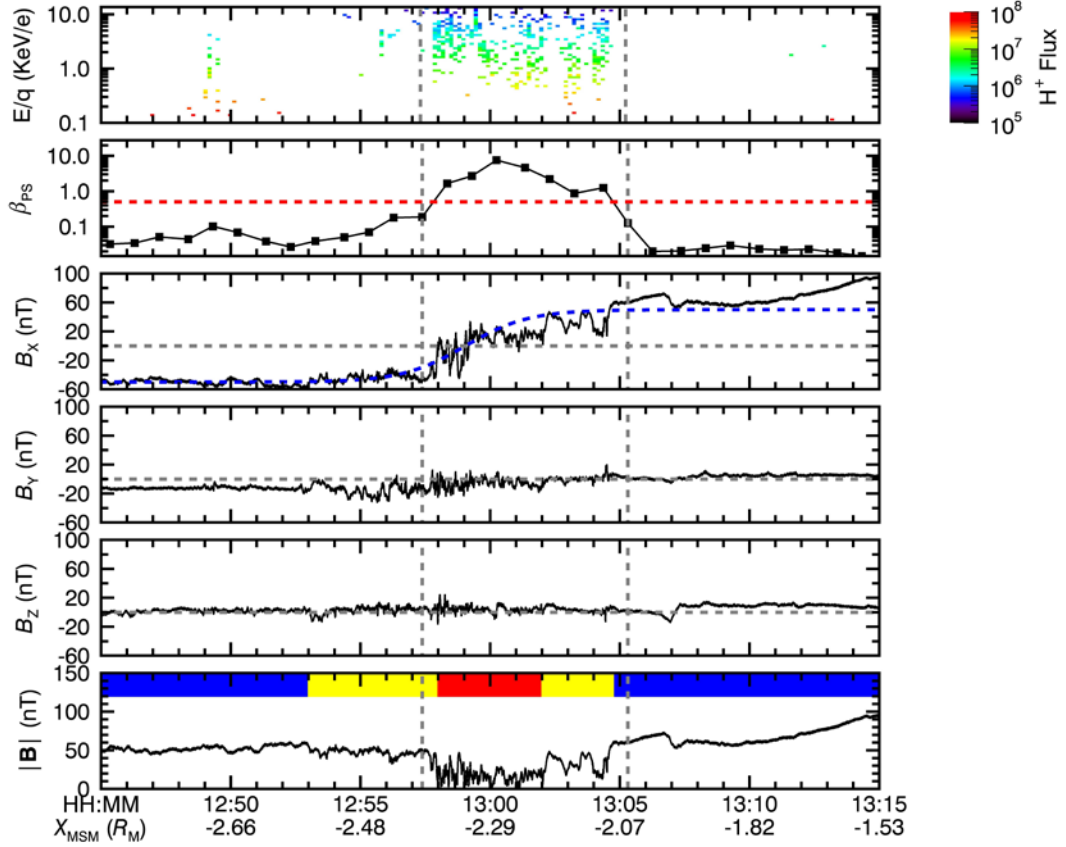


Figure 1: FIPS E/Q spectrogram (Panel 1), plasma β (Panel 2) and magnetic field (Panel 3 – 6) measurements of MESSENGER crossing of Mercury’s PS on February 18th 2012. Panel 3 shows the fitted Harris current sheet. Red, blue and yellow color bars represent the PS, PSBL and tail lobe (northern/southern) regions, respectively. Vertical lines represent the PS interval identified using the criteria $\beta \geq 0.5$.

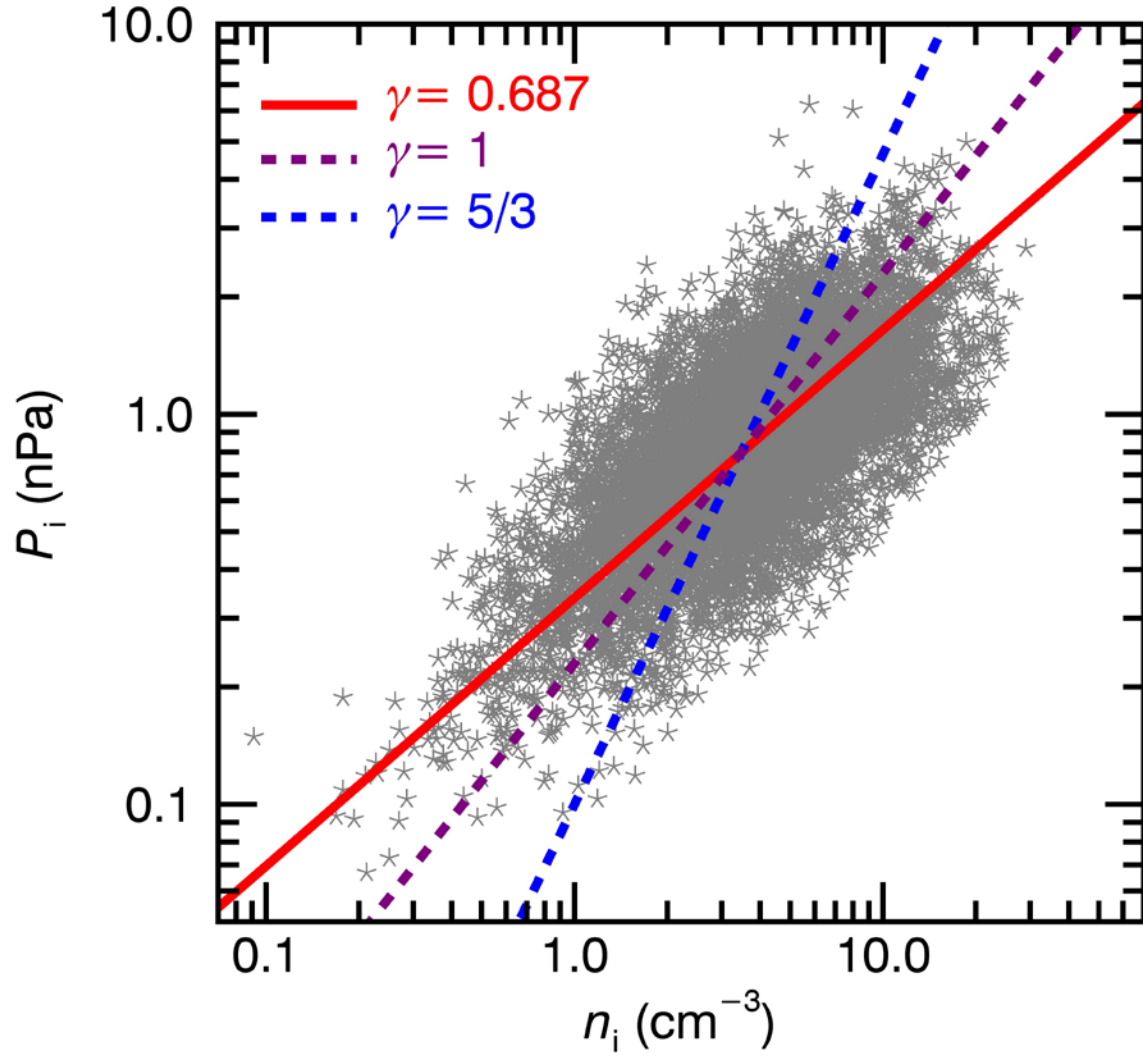


Figure 2: Logarithmic values of P_i vs. n_i measured in 759 Mercury's PS crossings. The red line represents the orthogonal regression line. The purple and blue lines represents the P_i vs. n_i relationship for $\gamma = 1$ (isothermal) and $5/3$ (adiabatic).

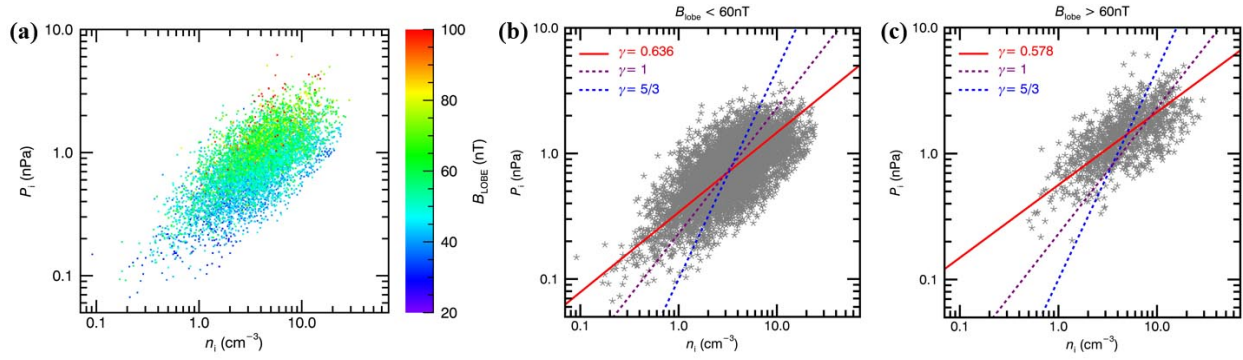


Figure 3: (a) Logarithmic values of P_i vs. n_i measurements. Colors represents average magnetic field intensity of Mercury’s tail lobe for each PS encounter. P_i vs. n_i measurements during (b) active and (c) quiet time.

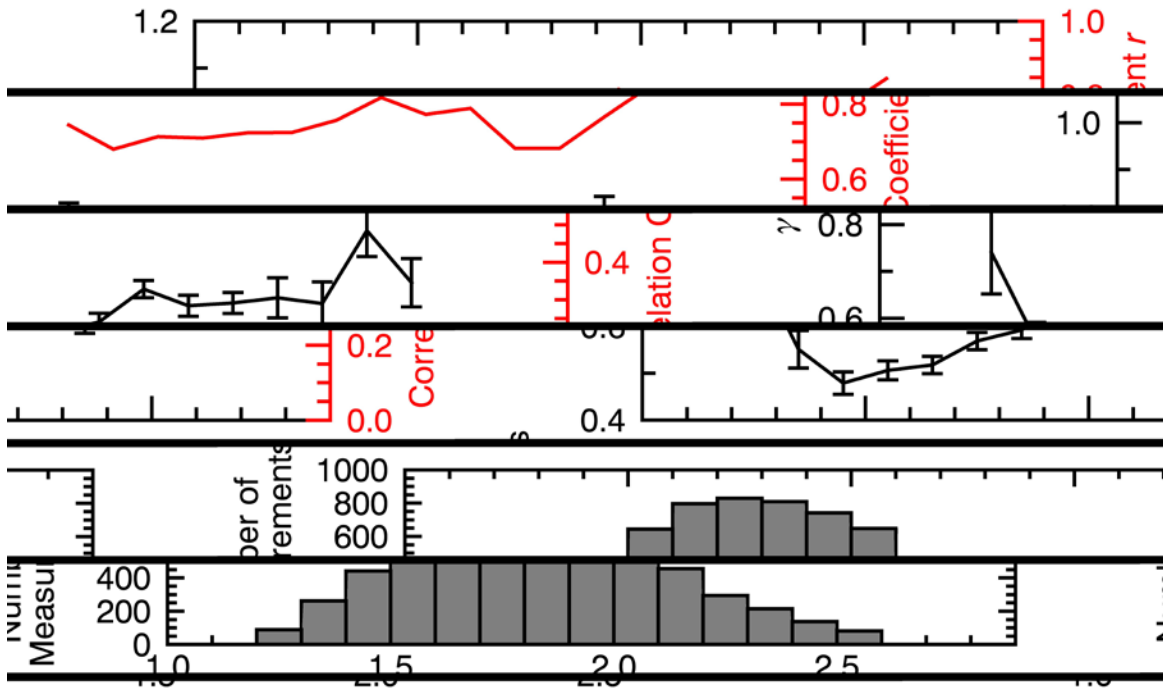


Figure 4: (top) Polytropic index γ and corresponding r versus radial distance R . P_i vs. n_i measurements are sorted into bins of $0.1 R_M$ from $R = 1.2$ to $2.6 R_M$. (bottom) Histogram of number of measurements in each bins.

References

- Anderson, B. J., M. H. Acuña, D. A. Lohr, J. Scheifele, A. Raval, H. Korth, and J. A. Slavin (2007), The Magnetometer instrument on MESSENGER, *Space Sci. Rev.*, 131, 417–450, doi:[10.1007/s11214-007-9246-7](https://doi.org/10.1007/s11214-007-9246-7).
- Anderson, B. J., C. L. Johnson, H. Korth, M. E. Purucker, R. M. Winslow, J. A. Slavin, S. C. Solomon, R. L. McNutt Jr., J. M. Raines, and T. H. Zurbuchen (2011), The global magnetic field of Mercury from MESSENGER orbital observations, *Science*, 333, 1859–1862, doi:[10.1126/science.1211001](https://doi.org/10.1126/science.1211001).
- Anderson, B. J., C. L. Johnson, and H. Korth (2013), A magnetic disturbance index for Mercury's magnetic field derived from MESSENGER Magnetometer data, *Geochem. Geophys. Geosyst.*, 14, 3875–3886, doi: 10.1002/ggge.20242
- Andrews, G. B., et al. (2007), The Energetic Particle and Plasma Spectrometer instrument on the MESSENGER spacecraft, *Space Sci. Rev.*, 131, 523–556, doi:[10.1007/s11214-007-9272-5](https://doi.org/10.1007/s11214-007-9272-5).
- Angelopoulos, V., C. F. Kennel, F. V. Coroniti, R. Pellat, M. G. Kivelson, R. J. Walker, C. T. Russell, W. Baumjohann, W. C. Feldman, and J. T. Gosling (1994), Statistical characteristics of bursty bulk flow events, *J. Geophys. Res.*, 99(A11), 21257–21280, doi: 10.1029/94JA01263.
- Baumjohann, W., and G. Paschmann (1989), Determination of the polytropic index in the plasma sheet, *Geophys. Res. Lett.*, 16, 295–298, doi:10.1029/GL016i004p00295.
- Baumjohann, W., and R. A. Treumann (1996), *Basic Space Plasma Physics*, 329 pp., Imperial Coll. Press, London.

Borovsky, J. E., M. F. Thomsen, and R. C. Elphic (1998), The driving of the plasma sheet by the solar wind, *J. Geophys. Res.*, **103**, 17,617–17,639.

Büchner, J., and L. M. Zelenyi (1989), Regular and chaotic charged particle motion in magnetotail-like field reversals: 1. Basic theory of trapped motion, *J. Geophys. Res.*, 94(A9), 11821–11842, doi:10.1029/JA094iA09p11821.

Chappell, C. R., T. E. Moore, and J. H. Waite Jr. (1987), The ionosphere as a fully adequate source of plasma for the Earth's magnetosphere, *J. Geophys. Res.*, 92(A6), 5896–5910, doi:10.1029/JA092iA06p05896.

Chen, C. X., and R. A. Wolf (1993), Interpretation of high speed flows in the magnetotail, *Geophys. Res.*, **98**, 21,409–21,419.

Delcourt, D. C., J. S. Murphree, Jr., and T. E. Moore (1996), On the nonadiabatic precipitation of ions from the near Earth plasma sheet, *Earth and Planetary Science Letters*, 141(A8), 17409–17418, doi:10.1029/96JA01006.

Delcourt, D. C., S. Grimald, F. Leblanc, J. M. Berthelier, and T. E. Moore (2003), A quantitative model of planetary Na⁺ contribution to Mercury's magnetosphere, *Ann. Geophys.*, **21**, 1723–1736, doi:10.5194/angeo-21-1723-2003

Deming, W. E. (1943). *Statistical Adjustment of Data*, New York: Wiley.

Dewey, R. M., Slavin, J. A., Raines, J. M., Baker, D. N., & Lawrence, D. J. (2017). Energetic electron acceleration and injection during dipolarization events in Mercury's magnetotail. *Journal of Geophysical Research: Space Physics*, 122, 12,170–12,188. <https://doi.org/10.1002/2017JA024617>

DiBraccio, G. A., J. A. Slavin, S. A. Boardsen, B. J. Anderson, H. Korth, T. H. Zurbuchen, J. M. Raines, D. N. Baker, R. L. McNutt Jr., and S. C. Solomon (2013), MESSENGER observations of magnetopause structure and dynamics at Mercury, *J. Geophys. Res. Space Physics*, 118, 997–1008, doi: 10.1002/jgra.50123.

DiBraccio, G. A., J. A. Slavin, J. M. Raines, D. J. Gershman, P. J. Tracy, S. A. Boardsen, T. H. Zurbuchen, B. J. Anderson, H. Korth, R. L. Jr. McNutt, et al. (2015a), First observations of Mercury's plasma mantle by MESSENGER, *Geophys. Res. Lett.*, 42, 9666–9675, doi: 10.1002/2015GL065805.

DiBraccio, G. A., et al. (2015b), MESSENGER Observations of flux ropes in Mercury's magnetotail, *Planet. Space Sci.*, 115, 77 – 89, doi:10.1016/j.pss.2014.12.016.

Erickson, G. M. and Wolf, R. A. (1980), Is steady convection possible in the Earth's magnetotail?. *Geophys. Res. Lett.*, 7: 897-900. doi:10.1029/GL007i011p00897

Frühauff D., Mieth J. Z. D. and Glassmeier, K. H., (2017) Average plasma sheet polytropic index as observed by THEMIS, *Annales Geophysicae*, **35**, 2, (253).

Gershman, D. J., J. A. Slavin, J. M. Raines, T. H. Zurbuchen, B. J. Anderson, H. Korth, D. N. Baker, and S. C. Solomon (2013), Magnetic flux pileup and plasma depletion in Mercury's subsolar magnetosheath, *J. Geophys. Res. Space Physics*, 118, 7181–7199, doi: 10.1002/2013JA019244.

Gershman, D. J., J. A. Slavin, J. M. Raines, T. H. Zurbuchen, B. J. Anderson, H. Korth, D. N. Baker, and S. C. Solomon (2014), Ion kinetic properties in Mercury's pre-midnight plasma sheet, *Geophys. Res. Lett.*, 41, 5740–5747, doi:10.1002/2014GL060468.

Goldstein, B. E., S. T. Suess, and R. J. Walker (1981), Mercury: Magnetospheric processes and the atmospheric supply and loss rates, *J. Geophys. Res.*, 86(A7), 5485–5499, doi: 10.1029/JA086iA07p05485.

Huang, C. Y., C. K. Goertz, L. A. Frank, and G. Rostoker (1989), Observational determination of the adiabatic index in the quiet time plasma sheet, *Geophys. Res. Lett.*, **16**, 563–566.

Imber, S. M., & Slavin, J. A. (2017). MESSENGER observations of magnetotail loading and unloading: Implications for substorms at Mercury. *Journal of Geophysical Research: Space Physics*, 122, 11,402–11,412. <https://doi.org/10.1002/2017JA024332>.

Jia, X., J. A. Slavin, T. I. Gombosi, L. K. S. Daldorff, G. Toth, and B. van der Holst (2015), Global MHD simulations of Mercury's magnetosphere with coupled planetary interior: Induction effect of the planetary conducting core on the global interaction. *J. Geophys. Res. Space Physics*, 120, 4763–4775. doi:10.1002/2015JA021143.

Kivelson, M. G., and H. E. Spence (1988), On the possibility of quasi quiet magnetotail, *Geophys. Res. Lett.*, **15**, 1541–1544.

static convection in

Korth, H., B. J. Anderson, D. J. Gershman, J. M. Raines, J. A. Slavin, T. H. Zurbuchen, S. C. Solomon, and R. L. McNutt Jr. (2014), Plasma distribution in Mercury's magnetosphere

derived from MESSENGER Magnetometer and Fast Imaging Plasma Spectrometer observations, *J. Geophys. Res. Space Physics*, 119, 2917–2932, doi: 10.1002/2013JA019567.

Linnet K., (1990) Estimation of the linear relationship between the measurements of two methods with proportional errors. *Stat Med*, **9**:1463-1473.

Orsini, S., et al. (2010), SERENA: A suite of four instruments (ELENA, STROFIO, PICAM and MIPA) on board BepiColombo -MPO for particle detection in t environment, *Planet. Space Sci.*, **58**, 166–181, doi:10.1016/j.pss.2008.09.012.

Pang, X., et al. (2015), *Sci. China Earth Sci.*, 58: 1993. <https://doi.org/10.1007/s11430-015-5122-6>.

Poh, G., J. A. Slavin, X. Jia, J. M. Raines, S. M. Imber, W. ~~D. S. Gershman~~, G. A. DiBraccio, K. J. Genestreti, and A. W. Smith (2017a), Mercury's cross -tail current sheet Structure, X ~~Geophysical Research Letters~~, **44**, 678–686, doi: 10.1002/2016GL071612.

Poh, G., J. A. Slavin, X. Jia, J. M. Raines, S. M. Imber, W. ~~D. S. Gershman~~, G. A. DiBraccio, K. J. Genestreti, and A. W. Smith (2017), Coupling between Mercury and its -tail current sheet formation, *J. Geophys. Res. Space Physics*, 122, 8419–8433, doi: 10.1002/2017JA024266.

Raines, J. M., J. A. Slavin, T. H. Zurbuchen, G. Gloeckler, B. J. Anderson, D. N. Baker, H. Korth, S. M. Krimigis, and R. L. McNutt Jr. (2011), MESSENGER Observations of the plasma environment near Mercury, *Planet. Space Sci.*, 59, 2004–2015, doi:10.1016/pss.2011.02.004.

Raines, J. M., D. J. Gershman, J. A. Slavin, T. H. Zurbuchen, H. Korth, B. J. Anderson, and S. C. Solomon (2014), Structure and dynamics of Mercury's magnetospheric cusp: MESSENGER measurements of protons and planetary ions, *J. Geophys. Res. Space Physics*, 119, 6587–6602, doi: 10.1002/2014JA020120.

Rong Z. J., Ding Y., Slavin J. A., Zhong J., Poh G., Sun W. J., Wei Y., Chai L. H., Wan W. X. and Shen C., (2018) The Magnetic Field Structure of Mercury's Magnetotail, *Journal of Geophysical Research: Space Physics*, **123**, 1, (548-566).

Saito, Y., J. ~~A. Sauvaud~~, M. ~~A. Sauvaud~~, and BepiColombo MMO/MPPE team (2010), Scientific objectives and instrumentation of Mercury Plasma Particle Experiment (MPPE) onboard MMO, *Planet. Space Sci.*, **58**, 182.

- Schindler, K., and J. Birn (1982), Self Earth's magnetotail, *J. Geophys. Res.*, **87**, 2263–2275. - consistent theor
- Sergeev, V. A., V. Angelopoulos, J. T. Gosling, C. A. Cattell, and C. T. Russell (1996), Detection of localized, plasma sheet, *J. Geophys. Res.*, 101(A5), 10817–10826, doi: 10.1029/96JA00460. - depleted flux t
- Shiokawa, K., W. Baumjohann, and G. Haerendel (1997), Braking of high-speed flows in the near-Earth tail, *Geophys. Res. Lett.*, **24**, 1179–1182, doi:10.1029/97GL01062.
- Siscoe, G. L. (1983), Solar system magnetohydrodynamics, in *Solar - Terrestrial Physics, Principles and Theoretical Foundations*, edited by R. L. Carovillano, and J. M. Forbes, pp. 11–100, D. Reidel, Hingham, Mass.
- Slavin, J. A., E. J. Smith, D. G. Sibeck, D. N. Baker, R. D. Zwickl, and S.-I. Akasofu (1985), An ISEE 3 study of average and substorm conditions in the distant magnetotail, *J. Geophys. Res.*, **90**, 10,875–10,895.
- Slavin, J. A., et al. (2009), MESSENGER observations of magnetic reconnection in Mercury's magnetosphere, *Science*, **324**, 606–610, doi:10.1126/science.1172011.
- Slavin, J. A., et al. (2010), MESSENGER observations of extreme loading and unloading of Mercury's magnetic tail, *Science*, **329**, 665–668, doi:10.1126/science.1188067.
- Slavin, J. A., et al. (2012), MESSENGER and Mariner 10 flyby observations of magnetotail structure and dynamics at Mercury, *J. Geophys. Res.*, **117**, A01215, doi:10.1029/2011JA016900.
- Smith, A. W., J. A. Slavin, C. M. Jackman, R. C. Fear, G. ~~K. Rodi~~ Braccio, J. M. Jasinski, and L. Trenchi (2017), Automated force ~~free flux~~ identification *Res. Space Physics*, **122**, 780–791, doi: 10.1002/2016JA022994.
- Spence, H. E., M. G. Kivelson, R. J. Walker, and D. J. McComas (1989), Magnetospheric plasma pressures in the midnight meridian: Observations from 2.5 to 35 R_E , *J. Geophys. Res.*, **94**(A5), 5264–5272, doi:10.1029/JA094iA05p05264.
- Sun, W.-J., J. A. Slavin, S. Fu, J. M. Raines, Q.-G. Zong, S. M. Imber, Q. Shi, Z. Yao, G. Poh, D. J. Gershman, Z. Pu, T. Sundberg, B. J. Anderson, H. Korth, and D. N. Baker (2015),

MESSENGER observations of magnetospheric substorm activity in Mercury's near magnetotail. *Geophys. Res. Lett.*, 42, 3692–3699. doi: 10.1002/2015GL064052.

Sun, W. J., S. Y. Fu, J. A. Slavin, J. M. Raines, Q. G. Zong, G. K. Poh, and T. H. Zurbuchen (2016), Spatial distribution of Mercury's flux ropes and reconnection fronts: MESSENGER observations, *J. Geophys. Res. Space Physics*, 121, 7590–7607, doi:10.1002/2016JA022787.

Sun W. J., J. M. Raines, S. Y. Fu, J. A. Slavin, Y. Wei, G. K. Poh, Z. Y. Pu, Z. H. Yao, Q. G. Zong, and W. X. Wan (2017), MESSENGER observations of the energization and heating of protons in the near ~~Mercury's magnetotail~~, *Mercury's magnetotail*, 44, 8149–8158, doi: 10.1002/2017GL074276.

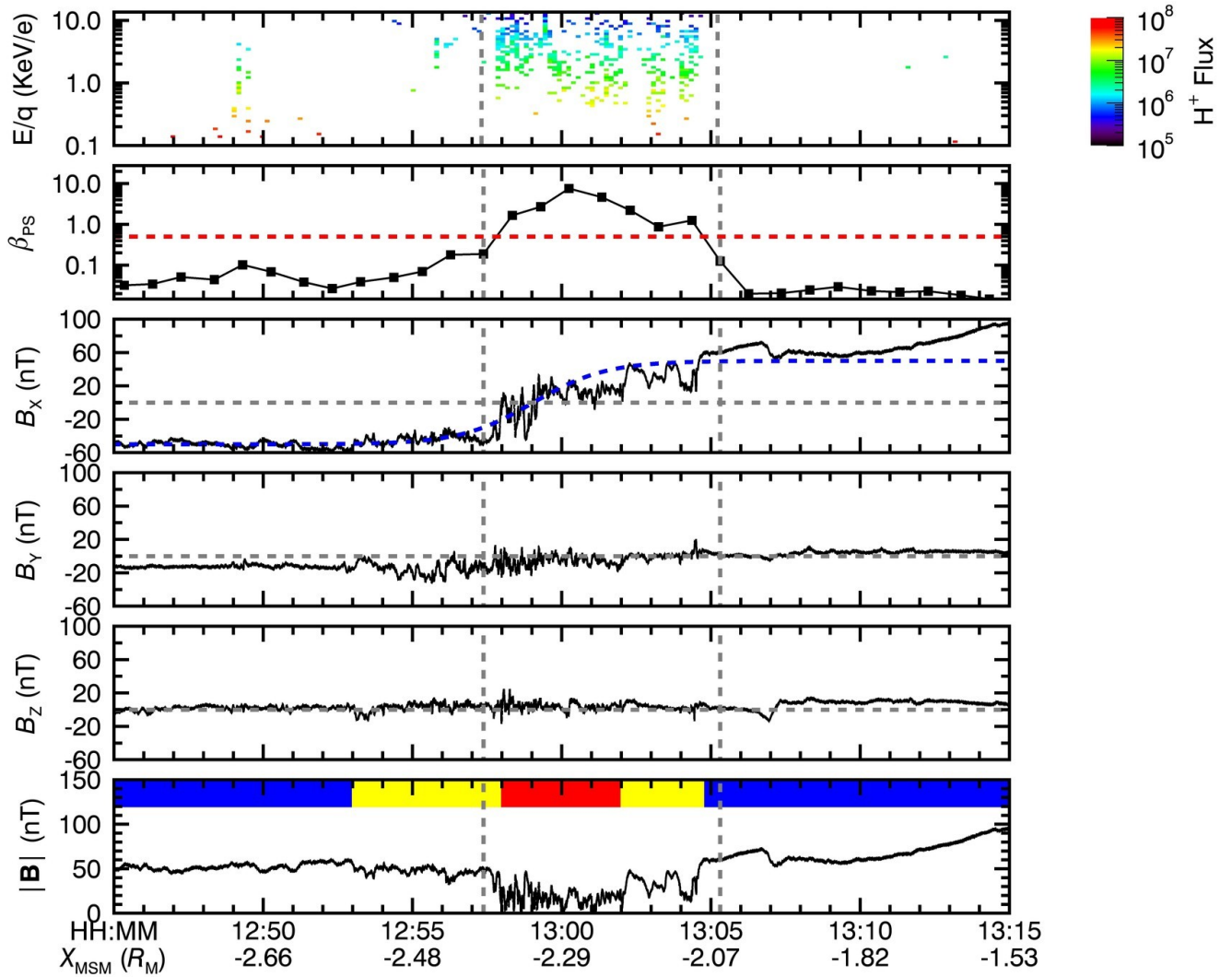
Sun, W. J., Slavin, J. A., Dewey, R. M., Raines, J. M., Fu, S. Y., Wei, Y., et al. (2018). A comparative study of the proton properties of magnetospheric substorms at Earth and Mercury in the near magnetotail. *Geophysical Research Letters*, 45. <https://doi.org/10.1029/2018GL079181>

Sundberg, T., et al. (2012), MESSENGER observations of dipolarization events in Mercury's magnetotail, *J. Geophys. Res.*, 117, A00M03, doi:10.1029/2012JA017756.

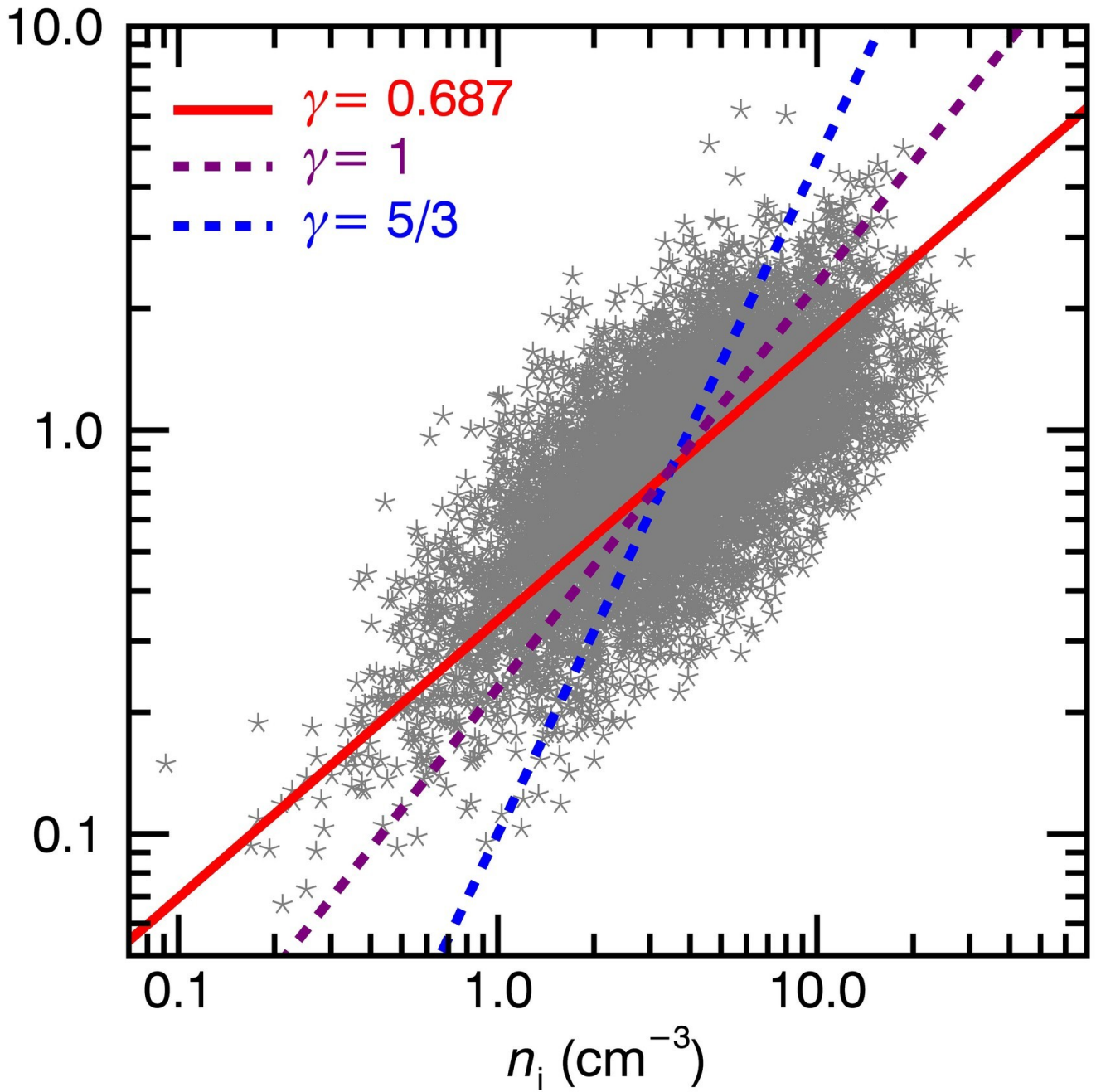
Zelenyi, L., M. Oka, H. Malova, M. Fujimoto, D. Delcourt, and W. Baumjohann (2007), Particle acceleration in Mercury's magnetosphere, *Space Sci. Rev.*, 132, 593–609, doi:10.1007/s11214-007-9169-3.

Zhong J., Wei Y., Pu Z. Y., Wang X. G., Wan W. X., Slavin J. A., Cao X., Raines J. M., Zhang H., Xiao C. J., A. M. Du, Wang R. S., Dewey R. M., Chai L. H., Rong Z. J. and Li Y., (2018) MESSENGER Observations of Rapid and Impulsive Magnetic Reconnection in Mercury's Magnetotail, *The Astrophysical Journal*, 10.3847/2041-8213/aaca92, **860**, 2, (L20).

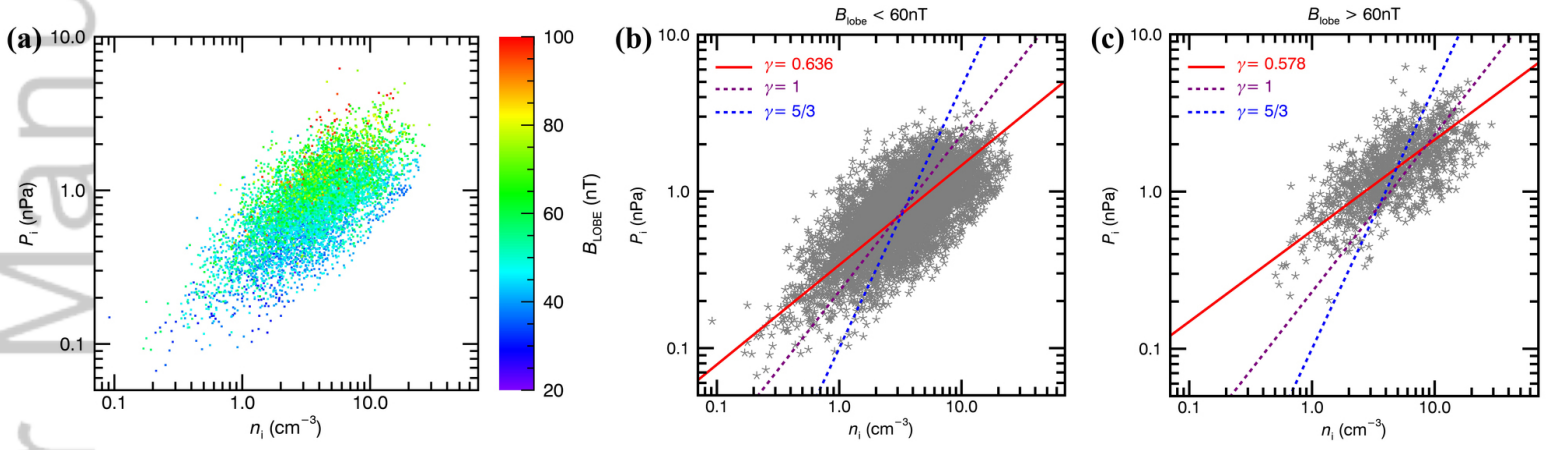
Zhu, X. M. (1990), Plasma sheet polytropic index as inferred from the FPE measurements, *Geophys. Res. Lett.*, **17**, 2321–2324.



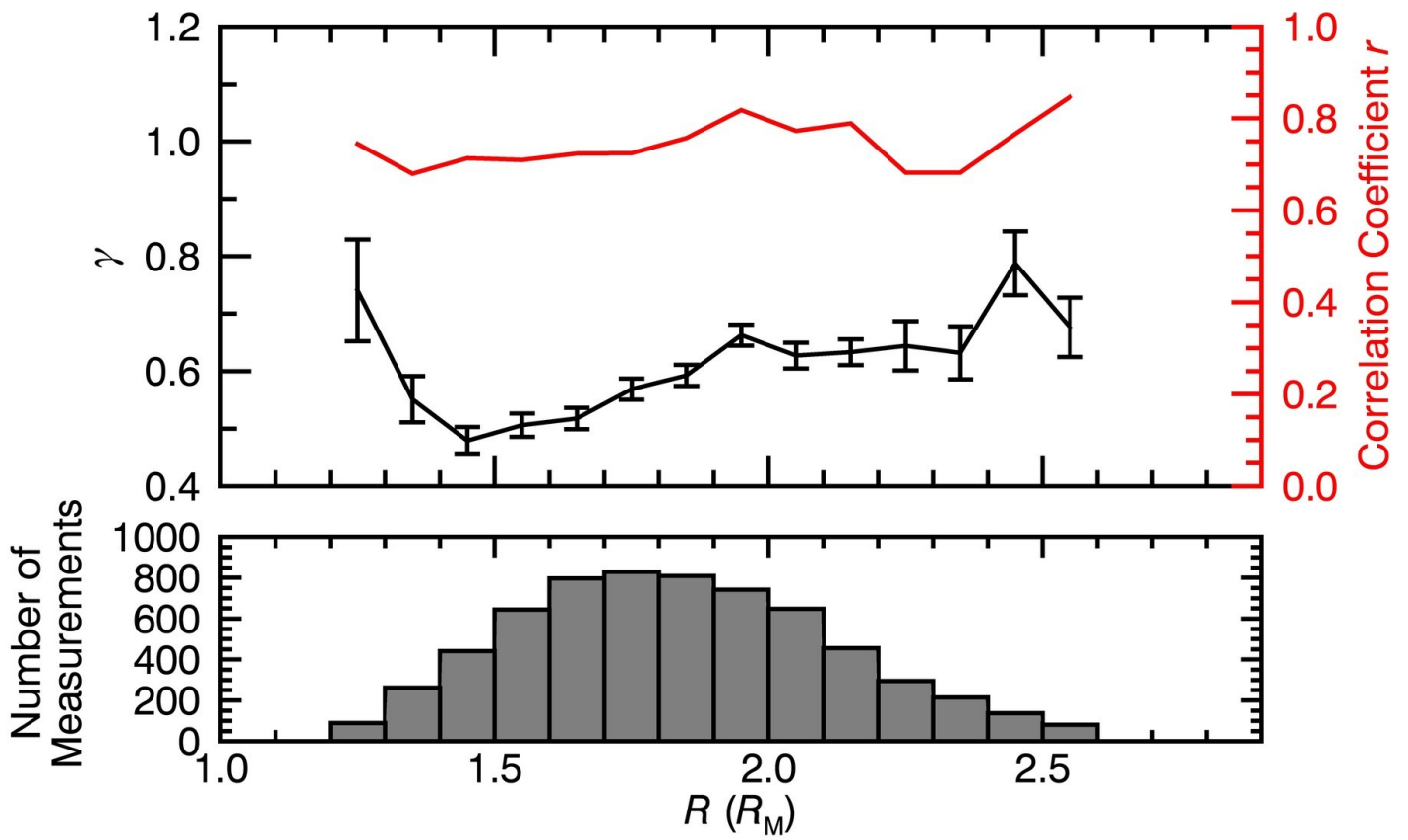
2018GL080601-f01-z-.jpg



2018GL080601-f02-z-.jpg



2018GL080601-f03-z-.jpg



2018GL080601-f04-z-.jpg